

A TROUBLESOME PAST: CHEMODYNAMICS OF THE FORNAX DWARF SPHEROIDAL

N.C. AMORISCO¹ AND N.W. EVANS¹

Institute of Astronomy, University of Cambridge, Madingley Road, Cambridge CB3 0HA, UK
Draft version February 15, 2018

ABSTRACT

We present compelling evidence for the complexity of the Fornax dwarf spheroidal. By disentangling three different stellar subpopulations in its red giant branch, we are able to study in detail the dependence between kinematics and metallicity. A well-defined ordering in velocity dispersion, spatial concentration, and metallicity is evident in the subpopulations. We also present evidence for a significant misalignment between the angular momentum vectors of the old and intermediate-age populations. According to the HST measurement of Fornax's proper motion, this corresponds to counter-rotation. These ingredients are used to construct a novel evolutionary history of the Fornax dwarf spheroidal, characterized as a late merger of a bound pair.

Subject headings: galaxies: kinematics and dynamics — Local Group — dwarf — individual: Fornax dwarf Spheroidal

1. INTRODUCTION

As the size and quality of datasets on the local population of dwarf Spheroidals (dSphs) increase, evidence for the complexity of these systems is intensifying. The observed variety of properties and structures gives each dwarf its own distinctive character. Their star formation histories, for instance, are well known to differ significantly. These often give rise to multiple generations of stars, but the mechanisms that drive an intermittent star formation must be investigated on a case-by-case basis. Being able to untangle the properties of such stellar subpopulations is crucial in advancing our understanding of how they came in place.

After the Sagittarius dwarf, Fornax is the second most luminous dSph orbiting the Milky Way and the only one (in addition to Sagittarius) to possess an associated Globular Cluster system (van den Bergh 1998). This is not Fornax's only peculiarity: for example, significant asymmetries in the isophotes were recorded as early as Hodge (1961), Eskridge (1988) and then confirmed in Irwin & Hatzidimitriou (1995). Recent deep photometric surveys (Stetson et al. 1998; Saviane et al. 2000; Battaglia et al. 2006, B06 in the following) have revealed a rich and prolonged star formation, comprising old stars ($\gtrsim 10$ Gyr), a dominant population of intermediate age stars, as well as stars of only a few hundred Myr.

All systematic studies of Fornax's star formation history (Coleman & de Jong 2008; Del Pino et al. 2011; de Boer et al. 2012) record a significant starburst at approximately 4 Gyr ago. The trigger of this activity, though, is still debated. On the one hand, at least three stellar overdensities have been identified in Fornax (Coleman et al. 2004, 2005; de Boer et al. 2012), and interpreted as reminiscent of the shell features observed in elliptical galaxies (Malin & Carter 1980). In this picture, Fornax collided with a low-mass sub-halo in the relatively recent past and swallowed it. On the other hand, the details are not free from difficulties, especially caused by the inferred metallicity and age of the stars composing the innermost clump (Olszewski et al. 2006;

Coleman & de Jong 2008). These are about 1.5 Gyr old, which makes the timing of the global starburst problematic. They are also relatively metal-rich, which in turn does not implicate an external origin for their gas. Furthermore, a recent collision is quite unlikely when the energetics of encounters in a virialized Milky Way halo is considered (De Rijcke et al. 2004).

After the pioneering work of Walker & Peñarrubia (2011) (WP11 in the following), in this *Letter*, we provide new evidence for Fornax's complexity by disentangling different stellar subpopulations in the red giant branch (RGB) and by studying in detail their kinematics. Rather than a division into two subpopulations (Saviane et al. 2000, B06, WP11), one into three is preferred by the data. The identified subpopulations show significant differences in line-of-sight (LOS) velocity dispersion and higher order moments. Even more striking is the incompatibility between their detected rotations, with the relative rotation vector inclined $\sim 40^\circ$ with respect to the isopotential major axis. Finally, we use these new ingredients to inform a novel formation scenario for the Fornax dSph.

2. THREE BAYESIAN SUBPOPULATIONS

A step forward in modelling the superposition of chemodynamically distinct stellar populations in dSphs has been achieved very recently by WP11. They devise a Bayesian technique that is able to quantify and separate the distributions of projected radii, velocities and metallicities of distinct subcomponents. Here, we use this technique extensively. Given a spectroscopic dataset, each star is associated to a set of probabilities of membership, one to each of the identified stellar subpopulations. This is useful, as it allows us to avoid any rigid color or metallicity cut, which inevitably degrades the data. Instead, these probabilities can be used in deriving robust and detailed kinematics for each subcomponent (e.g., Amorisco & Evans 2012, A12 in the following). Each population is assumed to have a Plummer surface density, a Gaussian metallicity distribution and a Gaussian LOS velocity distribution (the latter hypothesis is relaxed in Section 4). Also, this technique is able

to correct for the selection effects introduced by the spatial distribution of the spectroscopic sample, hence all inferred quantities – such as half-light radii and fractions of giants – are genuine global quantities.

WP11 apply this technique to the (approximately 2500) red giants in the Walker et al. (2009) spectroscopic dataset (W09 in the following), and look for a decomposition in, at most, two subcomponents. Indeed, they distinguish a dominant, colder and more concentrated metal-rich (MR) stellar population, from a more diffused, kinematically hotter metal-poor (MP) population. However, we reckon that such a division into two subpopulations is not stable with respect to removal of the kinematic information. If only the spatial distribution and the metallicities of the giants are used (i.e. discarding the LOS velocities), a different division is recovered. This is not the case if the presence of a third population is allowed, as shown in Table 1. In fact, a three-population division is a significantly better description: since the two models are nested, the comparison is straightforward and a simple maximum-likelihood ratio (MLR) is sufficient. Following Eadie et al. (1971), we find that despite the penalty given by the additional free parameters, the probability of obtaining such a MLR by pure chance is less than 3×10^{-6} . Additionally, no evidence is found in the data to justify the addition of a fourth population.

While the clear correlations between metallicity, spatial distribution and velocity dispersion are naturally maintained in passing from two to three subpopulations, the data prefer to accommodate separately a small fraction of MR giants, which in turn have colder kinematics and are more centrally concentrated. A division into three subpopulations also best traces Fornax’s star formation history, allowing at the same time for stars that are older and younger than the bulk of intermediate-metallicity (IM) giants. In this sense, the presence of such a feature can be easily understood, as the abundant 1-2 Gyr old population of stars, traced for example by the blue loop stars (B06 or de Boer et al. 2012), are also expected to sneak into the RGB.

The top panel of Fig. 1 shows the final metallicity subdivision of the W09 dataset. The MR peak is scarcely visible against the strong and broad IM population, whilst the middle panel shows the cumulative mass distributions of the three populations, illustrating the importance of combining evidence from the metallicity and the spatial distribution of the giants. A confirmation of the statistical importance of the MR feature comes from the independent spectroscopic dataset of B06. This has a different spatial distribution and contains at least 400 giants that do not appear in the W09 dataset. Furthermore, metallicities have been calibrated from spectra in the Ca II triplet region, and are affected by smaller uncertainties, resulting in a significantly less broadened metallicity distribution in the lower panel of Fig. 1. We apply the same statistical technique and again obtain that a division into three populations is a significantly better description (the probability of obtaining such a MLR by chance is $\lesssim 5 \times 10^{-4}$). The MR feature sits at $[\text{Fe}/\text{H}] \approx -0.65$, and is more concentrated than the other two subpopulations¹.

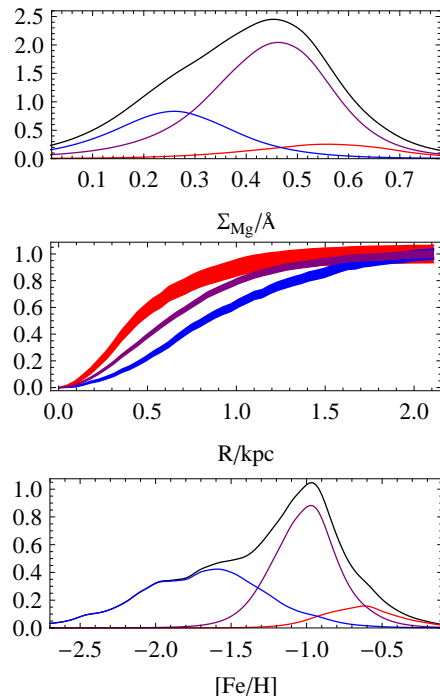


FIG. 1.— Upper and middle panels: metallicity distributions and cumulative mass distributions (one sigma errors) for the Walker et al. (2009) dataset. Lower panel: metallicity distributions for the Battaglia et al. (2006) dataset. Color-coding is associated with increasing metallicity.

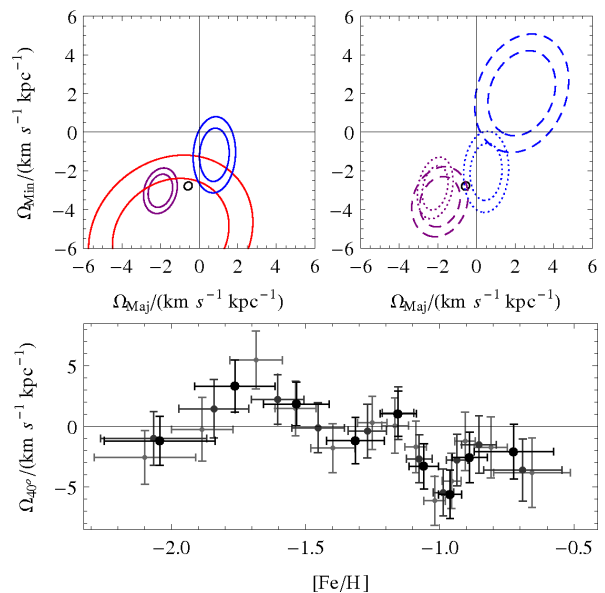


FIG. 2.— Top-left: rotation pattern from the datasets of Walker et al. (2009), one and two sigma contours for each stellar population, color-coding as in Fig. 1; in black, Fornax’s PM as from Piatek et al. (2007). Top-right: rotation for inner (dotted ellipses) and outer (dashed ellipses) stars for the IM and MP population. Lower panel: the intrinsic rotation signal (after subtraction of the PM) along the direction of the relative rotation, as a function of metallicity, for the Battaglia et al. (2006) dataset. Datapoints of growing sizes (and darker shades) are obtained from larger subsamples.

the three subpopulations as obtained from the B06 dataset. Unlike the metallicity, these are not reliable unless the spatial sampling bias is taken into account.

¹ We do not record information on the fractions or scale radii of

TABLE 1
TWO AND THREE POPULATION DIVISIONS OF THE FORNAX DWARF

Stellar Population	$\langle \Sigma_{\text{Mg}} \rangle$ [in \AA]	StD(Σ_{Mg}) [in \AA]	R_{h} [in pc]	Fraction of Population	$\langle \sigma \rangle$ [in kms^{-1}]
Metal-poor	0.31 ± 0.025	0.09 ± 0.015	860 ± 60	0.40 ± 0.09	14.4 ± 0.6
	0.24 ± 0.015	0.04 ± 0.015	1050 ± 90	0.19 ± 0.04	-
Metal-rich	0.47 ± 0.01	0.081 ± 0.005	556 ± 24	0.60 ± 0.09	10.0 ± 0.6
	0.447 ± 0.007	0.091 ± 0.004	598 ± 16	0.81 ± 0.04	-
Metal-poor	0.27 ± 0.018	0.07 ± 0.01	888 ± 50	0.31 ± 0.06	14.3 ± 0.6
	0.26 ± 0.015	0.05 ± 0.01	935 ± 65	0.27 ± 0.09	-
Intermediate	0.46 ± 0.01	0.058 ± 0.006	605 ± 30	0.56 ± 0.05	11.3 ± 0.7
	0.453 ± 0.009	0.065 ± 0.008	610 ± 25	0.63 ± 0.07	-
Metal-rich	0.53 ± 0.035	0.11 ± 0.02	480 ± 45	0.13 ± 0.04	8.6 ± 1
	0.56 ± 0.05	0.10 ± 0.025	437 ± 55	0.10 ± 0.04	-

NOTE. — Top-part: detailed results for a two-population division. Lower part: a third population is allowed. Results are collected for the case in which the kinematic information is retained (first line for each population), or discarded (second line).

3. A COMPLEX ROTATION PATTERN

Since Fornax is an extended object, those stars that are misaligned with the barycenter have their LOS velocities affected by a geometrical projection of the systemic proper motion (PM) (Feast et al. 1961). This projection is equivalent to an apparent solid-body rotation; hence, any rotation signal detected in the LOS velocities is actually the superposition of any *intrinsic* and *apparent* rotation:

$$\vec{\Omega}_{\text{tot}} = \vec{\Omega}_{\text{int}} + \vec{\Omega}_{\text{app}} , \quad (1)$$

where $\vec{\Omega}_{\text{app}}$ is proportional to the systemic PM $\vec{\mu}$ (e.g. eqn (3) in A12). For clarity, our frequencies are defined so that

$$v_{\text{los}}(x_{\text{Maj}}, x_{\text{Min}}) = \begin{pmatrix} \Omega_{\text{Maj}} \\ \Omega_{\text{Min}} \end{pmatrix} \cdot (x_{\text{Maj}}, x_{\text{Min}}) , \quad (2)$$

with all cartesian components referring to the major and minor axes of the isophotes.

Walker et al. (2008) have recently measured the total rotation signal in Fornax. They find it in agreement with the direct astrometric determination of Fornax’s PM, as obtained by Piatek et al. (2007, henceforth P07) using HST data. It was then natural to interpret this result as evidence that Fornax has very little intrinsic rotation in the LOS direction. Indeed, both the W09 and the B06 datasets are consistent with this interpretation, although this simple picture remains valid only as long as all the giants in each dataset are considered together. When we draw subsamples, we detect a strong dependence of the total rotation signal on metallicity, with a richness of detail that is surprising for such a small system.

In order to measure total LOS rotations $\vec{\Omega}_{\text{tot}}$, we adopt the same maximum-likelihood technique as in Walker et al. (2008). Our probabilities of membership allow us to measure the rotational properties of each subcomponent. As a compromise between size of the subsamples and excessive contamination, we only consider giants with at least 50% chance of belonging to a specified population, but our results are qualitatively stable against changes in this choice. Results are shown in Fig. 2.

The measure we obtain for the MR feature has a large uncertainty, due to the limited number of stars (≈ 80 giants with $p_{\text{MR}} > 0.5$), as well their spatial concentration. On the other hand, the rotations of the MP and the IM populations are precise enough to clearly detect

a *relative* rotation:

$$\vec{\Omega}_{\text{rel}} \equiv \vec{\Omega}_{\text{tot}}^{\text{IM}} - \vec{\Omega}_{\text{tot}}^{\text{MP}} = \vec{\Omega}_{\text{int}}^{\text{IM}} - \vec{\Omega}_{\text{int}}^{\text{MP}} . \quad (3)$$

This is inclined at $\sim 40^\circ$ with respect to the major axis and provides a natural justification to the angular behaviour of the asymmetries detected in the LOS velocity distribution by A12 (see their Fig. 12). Its magnitude is independent of the systemic PM and is non-negligible, amounting to at least $3 \text{ kms}^{-1} \text{ kpc}^{-1}$ – as a comparison, Fornax’s tidal radius is $\sim 2.85 \text{ kpc}$ (Irwin & Hatzidimitriou 1995). Furthermore, if we assume that the PM measured by P07 is correct, then this relative rotation is also a *counter*-rotation.

The B06 dataset confirms this picture. In fact, since their metallicities are more accurate, it provides an even more detailed description, as shown in the lower panel of Fig. 2. A comparison with Fig. 1 shows that peaks at positive and negative values of Ω_{40° trace the peaks in the metallicity distribution, respectively, of the MP and IM populations. Nonetheless, additional structure is also visible. The most significant lies in the MP end of the distribution, where the rotational velocity Ω_{40° drops again at negative values. This feature is in fact rather thought-provoking because it cannot be interpreted as an effect of contamination of the MP population from the other subpopulations. Still, it also appears in the W09 dataset. In fact, additional indications that the MP population may indeed have a richer structure come from the top-right panel of Fig. 2, in which the W09 subsamples pertaining to the IM and MP populations are split into two circular annuli each. While for the IM the innermost giants (dashed ellipses) share the same rotation as the outermost ones (dotted ellipses), we detect a significantly more pronounced relative rotation in the innermost MP giants (approximately within 1 kpc).

4. DISPERSIONS AND HIGHER ORDER MOMENTS

A12 have recently developed a Bayesian implementation for the extraction of the shape information of line profiles from discrete data. We apply that here and, for the first time, measure resolved kinematics of the stellar subpopulations in Fornax. It is probably worth mentioning that, in order to obtain reliable information on the higher order moments, it is necessary to use the results on the division into three populations as obtained by discarding the kinematic information (see Section 2).

The left panel of Figure 3 collects the velocity dispersions profiles – in circular annuli – for the three iden-

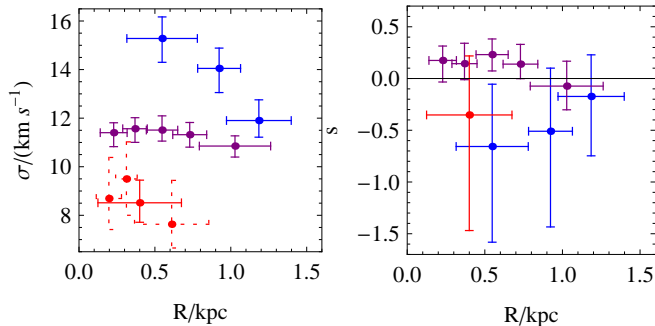


FIG. 3.— Velocity dispersion and symmetric deviations in circular annuli for the three stellar subpopulations.

tified subpopulations, with the same color-coding as in Fig. 1 (additional red-dotted points use a smaller bin-size for the MR population). It is reassuring to find that a Bayesian dissection only based on spatial positions and metallicities also yields significantly different kinematic profiles. In fact, also the shape of the velocity distributions shows significant differences. We recall that the symmetry parameter s is analogous to the Gauss-Hermite coefficient h_4 , and quantifies – with respect to a Gaussian ($s = 0$) – how ‘peaked’ ($s > 0$) or ‘flat-topped’ ($s < 0$) the velocity distributions is (see A12 for further details). A12 recorded a preference for a mild flat-toppedness in Fornax ($s \approx -0.3$), which we can now interpret as being due, at least in part, to the detected relative rotation. Instead, once isolated, the IM population prefers quasi-Gaussian profiles, with a mild tendency for positive values of s .

5. A MERGER OF A BOUND PAIR?

We have presented a detailed view of the rich kinematical properties of the apparently puny Fornax dSph. Both spectroscopic datasets (B06 and W09) support a Bayesian division into three populations of its RGB, with a new MR feature being identified at $[\text{Fe}/\text{H}] \approx -0.65$, containing approximately a tenth of the giants. Both datasets also show a strong dependence between stellar kinematics and metallicity. This includes a well-defined ordering of the three populations in velocity dispersion and spatial concentration, but it is most dramatic in a clear misalignment between the angular momentum vectors of the MP and the IM populations. The magnitude of this difference is independent of the systematic PM of Fornax, but, if we assume that the measurement by P07 is correct, then this misalignment also translates into a counter-rotation. The populations are then rotating in opposite directions along an axis inclined at $\sim 40^\circ$ with respect to the major axis.

Together with other evidence in the literature, the abundance of features complicates the task of a coherent reconstruction of Fornax’s evolutionary history. For instance, a merging scenario seems to be naturally invoked by the shell features present in the photometry (Coleman et al. 2004, 2005). Even so, this is made less convincing by the realization that the gas fueling the stars in such overdensities is more likely from Fornax itself, given its significant pre-enrichment (Olszewski et al. 2006; Coleman & de Jong 2008). Furthermore, the merger scenario has to overcome the difficulty of having a collision between two sub-haloes orbit-

ing the Milky Way at such late times (De Rijcke et al. 2004). On the other hand, it is almost impossible to reconcile the misalignment between the angular momenta of the MP and IM population without interactions. If we are skeptical about the PM measurement by P07, we might relax the argument for counter-rotation, and then invoke a tidal origin for the different rotational properties of the MP stellar population. Nonetheless, the fact that it is actually the innermost MP stars that have a faster relative rotation rather than the outermost ones argues against this, since those stars sit at the same distance from the center as most of the IM stars.

Furthermore, supporting evidence is provided by the fact that the spatial distribution of the youngest stars in Fornax seems to have knowledge of the direction of the relative rotation. Stetson et al. (1998) note that the main sequence stars “display a clearly flattened distribution on the sky, with a long axis in the east-west direction” (see their Fig. 12), hence in perfect alignment with $\vec{\Omega}_{\text{rel}}$. It is then appealing to advocate that this central structure, composed by stars that are younger than a few 100 Myr and whose geometry is uncorrelated with Fornax’s isophotes, is reminiscent of an elongated bar. If so, its spatial alignment is also the direction of its intrinsic rotational velocity. In turn, this is aligned with the intrinsic rotations of the MP and IM populations only if the PM is not significantly different from P07.

We suggest that a solution for these inconsistencies is that Fornax is a merger of a bound pair. First, if Fornax and its perturber have some relative orbital motion at early times, say with frequency $\vec{\Omega}_{\text{orb}}$, then interactions with the old MP population provides an efficient means of heating and preferentially stripping the progradely rotating stars (D’Onghia et al. 2010; Read et al. 2006). As a result, whatever the initial internal orbital structure, the MP population is left with a counter-rotating signature (with respect to $\vec{\Omega}_{\text{orb}}$). Second, the nearby presence of a companion increases significantly the chances of retaining the gas expelled by the first generations of stars in Fornax. Its escape is made more difficult by the increased total mass and by the gas-dynamics of the interactions with the companion. As dynamical friction eventually causes the decay of the perturber’s orbit, the infalling gas naturally has both a high metallicity and a prograde rotational signature, hence imprinted in the younger stellar populations. This process may be prolonged, and the localized overdensities (Coleman et al. 2004) and the central bar of main sequence stars may represent the last stages before the supply of gas is extinguished.

How massive might such a putative companion be? By assuming that the luminosity in the RGB is about one half of the total in Fornax, that the luminosity functions of the three sub-populations are the same, and that the metal poorest tail contains about one third of the MP giants, we get $L \approx 7 \times 10^5 L_\odot$, roughly comparable to Canes Venatici I, Draco, Sextans, Ursa Minor, although this may just be a lower limit. These dSphs have masses of $\approx 4 \times 10^7 M_\odot$ within 1.7 half light radii (e.g., Amorisco & Evans 2011), therefore probably more than a few $10^8 M_\odot$ in total. While this is still too low to make a late collision probable, it is instead enough to significantly perturb the progradely rotating stars in For-

nax, and to ensure an infall timescale of a fraction of the Hubble time. We conclude that this picture collects the benefits of the merging scenario while overcoming most of its limits.

NA thanks STFC and the Isaac Newton Trust for financial support. We thank Adriano Agnello, Giuseppe Bertin, Elena D’Onghia, Jorge Peñarrubia, Justin Read and Matthew Walker for inspiring conversations and useful criticism, as well as the referee, Mario Mateo, for helping us to improve the manuscript.

REFERENCES

- Amorisco, N. C., & Evans, N. W. 2011, *MNRAS*, 411, 2118
 Amorisco, N. C., Evans, N. W. 2012, *MNRAS*, in press, arXiv:1204.5181 (A12)
 Battaglia, G., Tolstoy, E., Helmi, A., et al. 2006, *A&A*, 459, 423 (B06)
 Coleman, M., Da Costa, G. S., Bland-Hawthorn, J., et al. 2004, *AJ*, 127, 832
 Coleman, M. G., Da Costa, G. S., Bland-Hawthorn, J., Freeman, K. C. 2005, *AJ*, 129, 1443
 Coleman, M. G., de Jong, J. T. A. 2008, *ApJ*, 685, 933
 de Boer, T., 2012, PhD thesis, University of Groningen
 Del Pino, A., Aparicio, A., Gallart, C., Hidalgo, S. 2011, *EAS Publications Series*, 48, 77
 De Rijcke, S., Dejonghe, H., Zeilinger, W. W., Hau, G. K. T. 2004, *A&A*, 426, 53
 D’Onghia, E., Vogelsberger, M., Faucher-Giguere, C.-A., Hernquist, L. 2010, *ApJ*, 725, 353
 Eadie, W. T., Drijard, D., James, F. E., Roos, M., Sadoulet, B. 1971, *Statistical Methods in Experimental Physics* Amsterdam: North-Holland, 1971,
 Eskridge, P. B. 1988, *AJ*, 96, 1614
 Feast, M. W., Thackeray, A. D., Wesselink, A. J. 1961, *MNRAS*, 122, 433
 Hodge, P. W. 1961, *AJ*, 66, 249
 Irwin, M., Hatzidimitriou, D. 1995, *MNRAS*, 277, 1354
 Malin, D. F., Carter, D. 1980, *Nature*, 285, 643
 Olszewski, E. W., Mateo, M., Harris, J., et al. 2006, *AJ*, 131, 912
 Piatek, S., Pryor, C., Bristow, P., et al. 2007, *AJ*, 133, 818 (P07)
 Read, J. I., Wilkinson, M. I., Evans, N. W., Gilmore, G., & Kleyna, J. T. 2006, *MNRAS*, 366, 429
 Saviane, I., Held, E. V., Bertelli, G. 2000, *A&A*, 355, 56
 Stetson, P. B., Hesser, J. E., Smecker-Hane, T. A. 1998, *PASP*, 110, 533
 van den Bergh, S. 1998, *ApJ*, 505, L127
 Walker, M. G., Mateo, M., Olszewski, E. W. 2008, *ApJ*, 688, L75
 Walker, M. G., Mateo, M., Olszewski, E. W. 2009, *AJ*, 137, 3100 (W09)
 Walker, M. G., Peñarrubia, J. 2011, *ApJ*, 742, 20 (WP11)